sustainability

MDPI

Article

Assessing the Prediction Accuracy of Frequency Ratio, Weight of Evidence, Shannon Entropy, and Information Value Methods for Landslide Susceptibility in the Siwalik Hills of Nepal

Bharat Prasad Bhandari [1], Subodh Dhakal [2,*] and Ching-Ying Tsou [3]

[1] Central Department of Environmental Science, Tribhuvan University, Kathmandu 44600, Nepal; bbhandari@cdes.edu.np
[2] Department of Geology, Tri-Chandra Multiple Campus, Tribhuvan University, Kathmandu 44600, Nepal
[3] Faculty of Agriculture and Life Science, Hirosaki University, Aomori 036-8561, Japan; tsou.chingying@hirosaki-u.ac.jp
* Correspondence: dhakalsubodh@gmail.com

Abstract: The main objective of this study is to assess the prediction and success rate based on bivariate frequency ratio (FR), weight of evidence (WoE), Shannon entropy (SE), and information value (IV) models for landslide susceptibility in the sedimentary terrain of Nepal Himalaya, as the area is facing threat for sustainable development as well as sustainable resource management. This study also seeks to evaluate the causative factors for landslide susceptibility. Initially, a landslide inventory map was created, consisting of 1158 polygons. These polygons were randomly divided into two sets, with a ratio of 70% for training and 30% for testing data. The multicollinearity approach was evaluated to assess the relevance of selected conditioning variables and their inclusion in the model construction process. The area under the curve (AUC) and other arithmetic evaluation methods were employed to validate and compare the outcomes of the models. In comparison, the predictive accuracy of the FR model surpasses that of the IV and SE models. The success rates, ranked in descending order, are as follows: WoE (79.9%), FR (75.3%), IV (74.4%), and SE (73.2%). Similarly, the success rates of four distinct models, namely WoE, FR, IV, and SE, are 85%, 78.75%, 78.57%, and 77.2%, correspondingly. All models have an accuracy and prediction rate exceeding 70%, making them suitable for assessing landslide susceptibility in the Siwalik Hills of Nepal. Nevertheless, the weight of evidence model provides more precise outcomes than other models. This study is expected to provide important information for road and settlement sustainability in the study area.

Keywords: landslide susceptibility; bivariate models; Siwalik Hills; model comparison

Citation: Bhandari, B.P.; Dhakal, S.; Tsou, C.-Y. Assessing the Prediction Accuracy of Frequency Ratio, Weight of Evidence, Shannon Entropy, and Information Value Methods for Landslide Susceptibility in the Siwalik Hills of Nepal. *Sustainability* **2024**, *16*, 2092. https://doi.org/10.3390/su16052092

Academic Editor: Lucio Di Matteo

Received: 3 February 2024
Revised: 26 February 2024
Accepted: 29 February 2024
Published: 2 March 2024

1. Introduction

Landslides are a frequently occurring geological hazard in Nepal that causes extensive damage to the environment and poses a threat to human life in mountainous areas [1]. Landslide is a general term for the downslope movement of rock, sediment, or accumulated debris [2]. It is caused by various natural hazards or human activities, such as an earthquake, road construction, deforestation, or mineral exploration [3]. According to global landslide statistics, China, Colombia, India, Philippines, Peru, and Nepal have been highly affected by landslides in the last decade [4]. According to the Ministry of Home Affairs Nepal [5], 92 people died, 80 people were injured, and 1968 houses were affected in the year 2021, which caused USD 13,11,267 losses due to landslides in Nepal. Similarly, 15,866 landslides were marked from 2019 to 2021 in the Siwalik Hills of Nepal, causing the death of 30 people and destroying 142 houses. Within these years, USD 4,44,680 were lost by the country only in the Siwalik Hills of Nepal. Preparing precise and efficient landslide susceptibility maps can provide valuable assistance for disaster preventive and mitigation initiatives and ensure adequate public security. Consequently, landslides have become a

significant threat for sustainability to human lives and natural properties, even though several studies on landslide modeling have been published over the past few decades in Nepal [6]. In Nepal, slope deformations, mass movement, and landslides are frequent geodynamic phenomena [7]. The research area is mostly affected by natural landslides and is experiencing significant challenges in terms of sustainability related to development and resource management. There is a need for research in the Babai River watershed of Siwalik Hills that includes landslide susceptibility analysis and compares the accuracy of different models. Among the 1156 landslides, more than 700 new and reactivated landslides were recorded in the Babai River watershed of the Siwalik Zone before 2021 [8]. According to several conditioning criteria, a landslide susceptibility study provides the spatial distribution of possible landslide sites [9].

Various causative factors like topography, slope, failure mechanism, rainfall intensity, land cover, geological formation, rock strength, and many other elements can cause or regulate landslides. Various approaches and techniques have been used in landslide susceptibility mapping, according to the literature, including inventory-based methods [10], bivariate and multivariate statistics like logistic regression (LR), frequency ratio (FR), statistical index, cluster analysis, and artificial neural networks (ANNs) [11]. Due to their ability to provide more accurate landslide prediction, the bivariate statistical models, including the weight of evidence, frequency ratio, Shannon entropy, and statistical index models, are more popular and acceptable. These techniques can be compared to determine the most accurate approach. For accurate susceptibility mapping, various statistical methods, including weight of evidence or generalized additive models, and various approaches to multi-criteria decision analysis (MCDA), regression analysis, and fuzzy sets can also be used and contrasted [1]. However, the weight of evidence and frequency ratio, along with statistical index models, are simple and more accessible and have less error. This study assesses the prediction accuracy of four bivariate landslide susceptibility techniques: the weight of evidence (WoE), frequency ratio (FR), information value (IV), and Shannon entropy (SE) models in the Siwalik Hills of Nepal.

2. Study Area

The Babai River watershed is approached for the present study. The Babai River has major tributaries originating from the Siwalik Hills. It has some typical characteristics such as east–west trending, parallels with rock strikes, less interruption by humans, and forest covering more than 80% of the area. The total area is between 27°57′59.03″ N, 82°33′42.80″ E in the east, 28°28′30.14″ N, 81°28′30.14″ E in the west, 28°12′47.90″ N, 82°15′46.08″ in the north, and 28°01′03.89″ N, 82°12′39.61″ E in the south. After its development, it enters the flat Dun Valley and re-enters the Siwalik (Figure 1). The total catchment area of the Babai watershed is 1952 km^2 but, for the present study, only 1157 km^2 because the rest of the site is either Dun Valley or plain Terai.

The primary plant species in the research region is Soria Robusta and the climate is subtropical. The topography is characterized by hills that reach elevations ranging from 109 to 1550 m above mean sea level. The climate of the area is characterized by long dry and extended wet seasons. There is an excessive amount of overlap between the wet and dry seasons. Pre-monsoon, monsoon, and post-monsoon are the three monsoon phases that coincide with the longer wet seasons. April and May are regarded as the pre-monsoon period, whereas June, July, and August are known as the monsoon period. September and October are the post-monsoon season. On the other hand, compared to the rainy season, the dry season experiences much less frequent and moderate to low intensity rainfall [8]. In the winter, the temperature can drop below 0 °C, while, in the summer, it can raise above 40 °C. The rainy season is when most people expect significant and intense rains. From 1990 to 2022, the annual precipitation varies from 1750 to 3250 mm in the study region. The average yearly rainfall ranges from 1550 to 2470 mm only during the monsoon season. Over 85% of the yearly precipitation falls during the monsoon season.

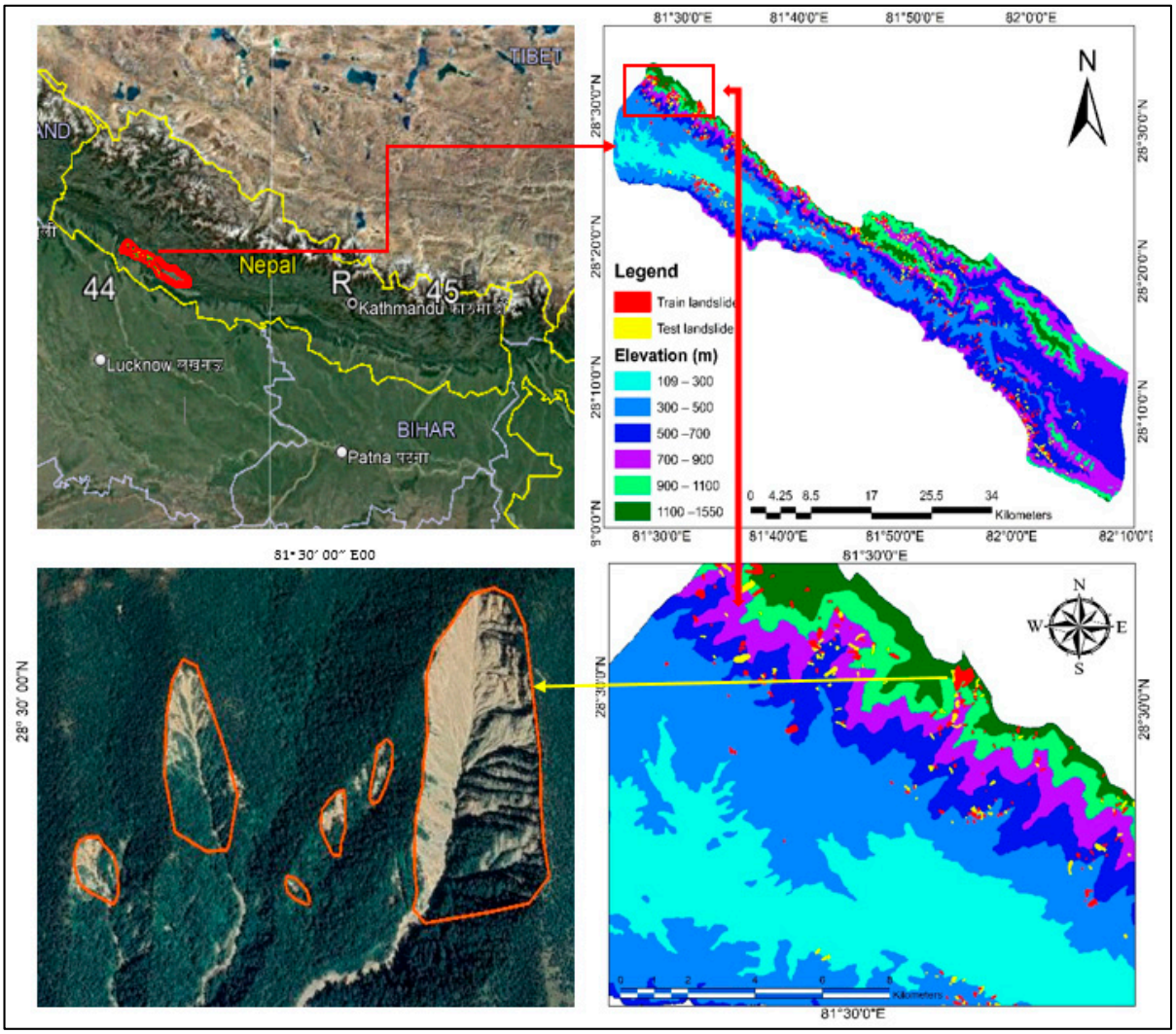

Figure 1. The study area's location map and landslide inventory map.

The Babai River flows in a direction parallel to the strike of the rocks and the hills and rills. The landforms are dynamic, constantly shifting, and evolving with time. Various processes, including the weathering of rocks, the continual erosion of weathered materials, landslides, and other mass movements, and the deposition of large masses of sediments, cause landform changes. In the area under investigation, tectonism is also responsible for the evolution of the landforms and the mass movement. The study area is characterized mainly by erosional and depositional landforms. The rough landscape, steep slopes, cliffs, and narrow ridges all contribute to the rapid erosion rate and the formation of gullies. The continual water discharge on a steep slope of weak sedimentary rocks caused the development of rock canyons and gorge. The debris flow fan, the talus cone, the bank deposits, and the river terraces are all common depositional landforms in the study region. Because of the several strata of rock masses, the area contains identical and distinct characteristics. The weathering pattern and rock fall mechanism are easily observable due to the alternating layers of weak and strong rocks. The examined area has intriguing geomorphological characteristics such as several hills, consecutive saddles, parallel hill chains, and numerous river valleys nestled between the narrow hills. The rocks of the study region were previously categorized into three geological units based on lithology and rock composition: Lower Siwalik, Middle Siwalik, and Upper Siwalik, from bottom to top, respectively. A recent Quaternary deposit covers the top of the stratigraphy. The Lower Siwalik comprises sandstone, mudstone, and a small amount of limestone in the

study area. The sandstone is medium to thickly bedded and fine- to medium-grained. The sandstones are interbedded with reddish-purple and greenish-grey shale (variegated mudstone). The shale is thinly bedded, predominately red, and laminated in the lower part of the Lower Siwalik.

The Middle Siwalik is well exposed in the study area. The Middle Siwalik in the study area comprises thickly bedded (>5 m), medium- to fine-grained sandstone interbedded with thickly bedded (>3 m) brownish-gray mudstone. The sandstones are greenish-gray in color, medium- to fine-grained, massive, and well jointed. The Upper Siwalik of Babai section comprises cobble and pebble-bearing conglomerate beds. Most of the conglomerates are cemented by clay components, whereas some beds are cemented by calcite. The boulder conglomerate beds are well exposed in the Babai Valley–Salyantari road section. A thin layer of brown mudstone and grey sandstone transitionally overlies the conglomerate beds. The boulders, cobbles, pebbles, and other sediments are derived from the Lesser and Higher Himalayas. The pebbles are well rounded to sub-rounded and made of quartzite, slate, and marble.

3. Methods

The overall method of this study is divided into four phases: desk study, field study, lab test, and data analysis. The field study includes landslide inventory map verification, geological map preparation, and causative factor verification. Desk study includes literature review, preparation of a spatial and temporal landslide inventory map, a geological map in GIS, extraction of DEM, and preparation of a landslide causative factor map. The research gaps were identified after conducting more than 200 literature reviews from index journals. The methodological framework of the study is given in the flow chart (Figure 2).

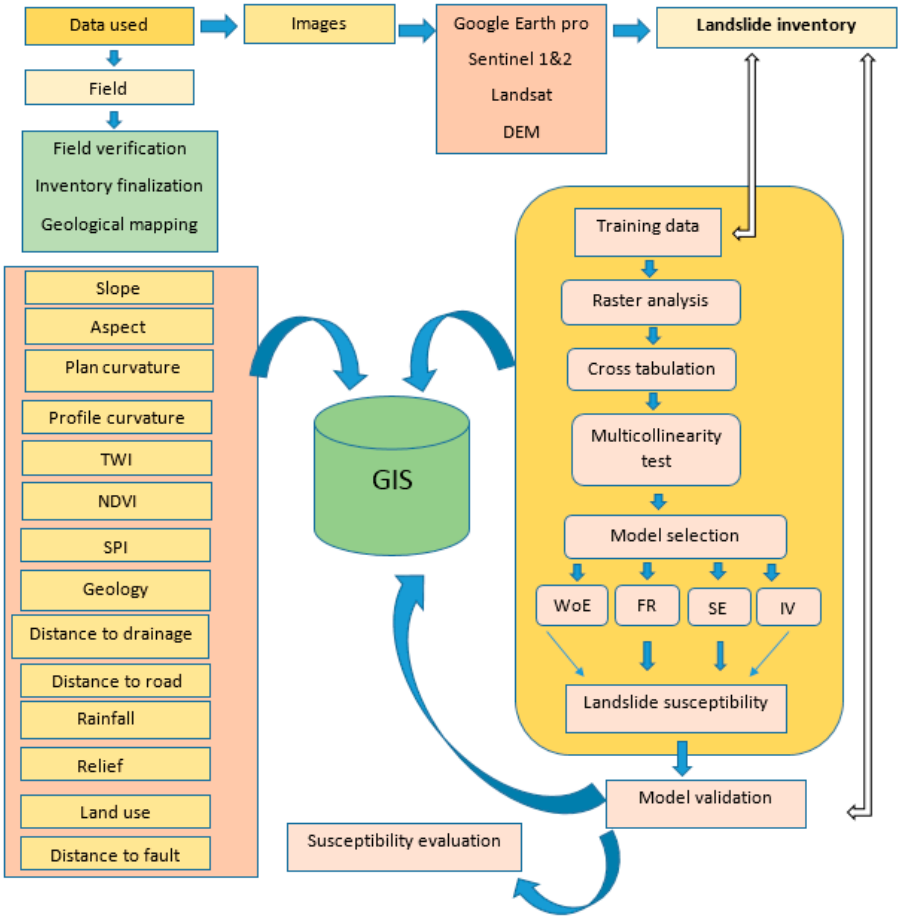

Figure 2. Methodological framework of landslide susceptibility mapping.

3.1. Preparation of Landslide Inventory Map

The work began with the identification of the landslide. The landslides can be spotted and plotted using satellite imagery or aerial photography [12]. However, in the hilly region of Nepal, it is rather challenging to capture explicit imagery using either technique due to dense vegetation and frequent cloud cover [13]. The training and test data were divided 70:30 depending on the geographical and temporal distribution of landslides in the research region. The landslides that occurred prior to 2019 were used as training data, whereas those that occurred after 2019 were used as testing data. The spatial and temporal landslide inventory map was created using the following steps: (a) every landslide was recognized and identified using images from Google Earth Pro, Landsat, and Sentinel-2,3. (b) The polygon tool was used to outline the landslide on the images and the resulting KML file was saved. (c) The KML file was retrieved from the GIS layer and the 1:10,000 scale map was prepared. (d) The prepared spatial and temporal inventory maps were validated on site. (e) Some landslides missing from the image were recorded with GPS data and then digitalized on the map.

3.2. Landslide Conditioning Factors

The selection of conditioning elements lacks precise and universally accepted rules, as it is contingent upon the availability of data sources. Similarly, the geo-environmental characteristics of the study region and the specific characteristics of landslides in that area are other vital factors for selecting landslide conditioning factors [1,14]. Based on geo-environmental conditions observed in the field and taking reference from the existing literature, 14 landslide conditioning factors, including slope (°), aspect, plan curvature, profile curvature, rainfall (average annual precipitation total in mm), stream power index (SPI), topographic wetness index (TWI), distance to drainage (m), lithology, distance to faults (m), distance to road (m), land cover, NDVI, and relative relief, were taken into consideration in the present study. With a geographical resolution of 30 m, the WGS-1984-UTM-Zone-45N projection system was used to process all of the thematic layers in GIS. The research region's digital elevation model (DEM) retrieved slope, aspect, curvature, topographical wetness index, and stream power index.

Multiple studies have used slope as a significant factor in determining the landslide susceptibility [15]. The aspect of a slope refers to its orientation. Multiple studies [16,17] have demonstrated a correlation between the slope aspect and the incidence of landslides. Different slope orientations, varying degrees of weathering, and fluctuating levels of moisture content are present [18]. Various studies have demonstrated that curvature has a significant role in the occurrence of landslides [19]. The topography of the terrain is characterized by overall curvature, which has a substantial influence on the occurrence of landslides. Chen et al. [20] state that the steepness of a slope can be estimated by the curvature of the plane, which is caused by the combination of the horizontal plane and surface landforms. The profile curvature refers to the vertical plane that is parallel to the direction of the slope [21]. Figure 3 displays the maps of slope, aspect, plan curvature, and profile curvature, labeled as a, b, c, and d, respectively.

The topographical wetness index quantifies the amount of accumulated flow at a specific location. The topographic wetness index (*TWI*) exerts significant influence on hydrological processes. It somehow depicts the distribution of moisture in the soil. The TWI quantifies the level of flow accumulation at a specific location within the study region, as shown in Figure 4a. The *TWI* partially reflects the dispersion of soil moisture.

$$TWI = ln\,(AS \div tan\beta)$$

According to Pradhan and Kim [22], the stream power index (*SPI*) is a crucial factor that quantifies the erosive force of water flow and sediment carried by water flow over land.

The stream power index map is shown in the Figure 4b. The DEM is utilized to ascertain the slope gradient and slope contributing area (AS) for the calculation of the SPI.

$$SPI = AS \times tan\beta$$

where AS is the slope contributing area and β is the slope angle.

The processing of Landsat-8 images in the GIS software (Version 10.6) obtained an NDVI map. A higher NDVI indicates more vegetation cover and a stable slope; however, a higher NDVI may lead to more landslides on the rocky slope covered with thick vegetation (Figure 5a).

$$NDVI = \frac{B5 - B4}{B5 + B4}$$

where $B5$ is near infra-red (NIR) and $B4$ is a red band.

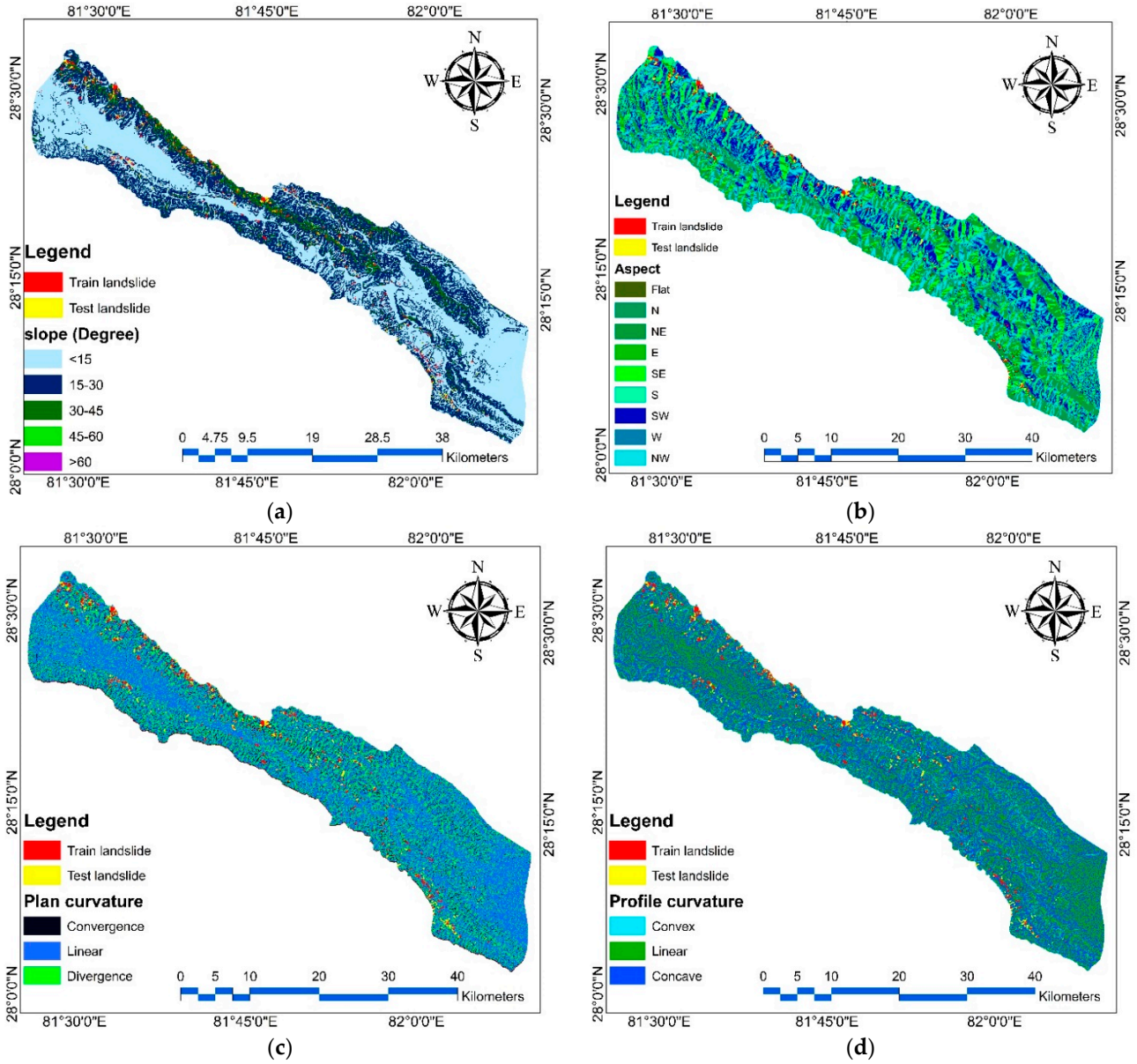

Figure 3. Landslide causative factor maps: (**a**) slope, (**b**) aspect, (**c**) plan curvature, (**d**) profile curvature.

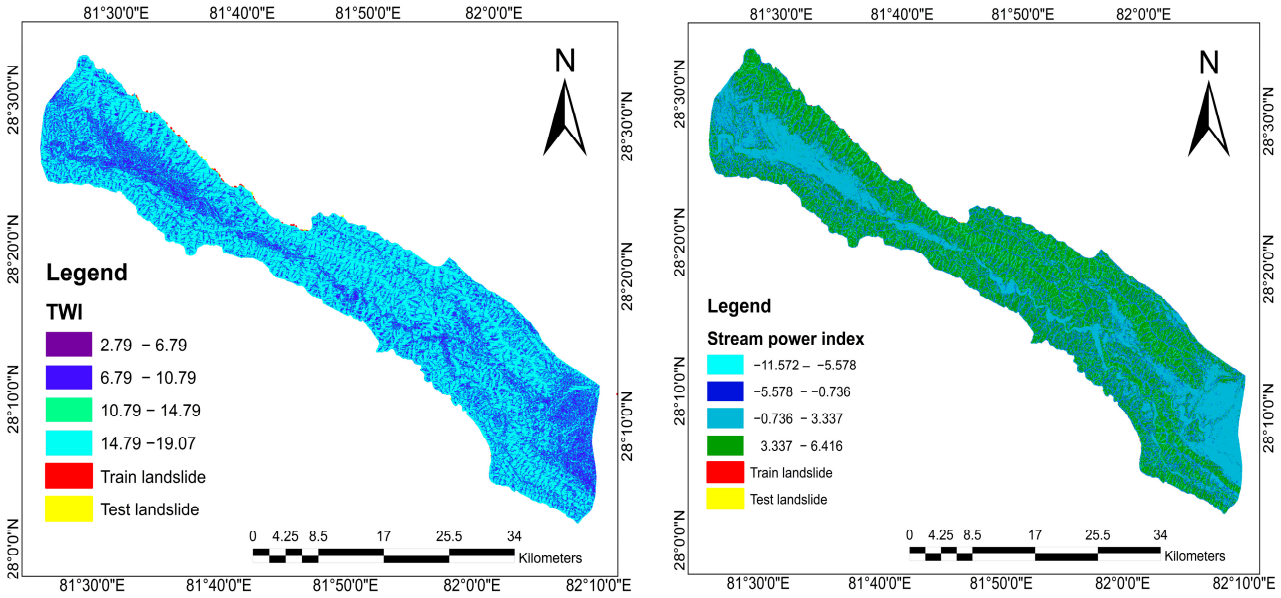

Figure 4. (**a**) Topographical wetness index. (**b**) Stream power index map.

The mechanism and distribution of landslides are heavily influenced by land cover. The global data show that the landslide distribution is higher in barren land. The root systems of the plants provide strong mechanical support, which plays a significant role in slope stabilization [23]. The land cover map was obtained from Landsat-8 imageries after processing in ArcGIS (Figure 5b). Rainfall is one of the most important extrinsic factors that can start a landslide, so Dahal et al. [24] used mean annual rainfall to measure landslide susceptibility. The rainfall map was obtained from 30-year average annual rainfall data from seven stations (Figure 5c). Relief is the difference between a particular surface's highest and lowest altitudes. The relative relief is derived from the digital elevation model. It was extracted by using Neighborhood and Raster Calculator in the GIS software (Figure 5d).

The rock types, composition, and combination were considered for the geological mapping. The strike and dip amount of the bedrock outcrop were plotted in the topographical map of the respective area. The draft map prepared in the field was digitized in the GIS layer and the final map of a 1:10,000 scale obtained (Figure 6a). Lithology and the slope of the surface determine the nature and intensity of a landslide [15].

The fault planes were identified in the field after rigorous geological study. The fault lines were traced out on the map. The polygon shapefile was converted into a raster. Using a spatial analysis tool in GIS, distances to the fault were divided into six buffer zones at 500 m intervals (Figure 6b). The effects of the fault can be seen from a far distance, so the distance to the fault was taken at an interval of 500 m. Streams make the slope unstable when it has a high-water discharge. A stream may have a higher slope and cause toe cuts, side erosion, and deposition. Similarly, the stream increases the infiltration rate and makes the ground saturated. The area near the river and streams is mostly wet and water-saturated, which increases landslide susceptibility [25]. The distance to drainage map was obtained from the digital elevation model of 30 m resolution (Figure 6c). The development of roads, railways, and trails in mountainous terrain mostly leads to slope instability and landslides [26]. In the mountains of Nepal, haphazard road construction leads to landslide mechanisms. The rocks of the Siwalik are weak, fragile, highly ruptured, and naturally unstable. Constructing the road on such terrain ultimately causes several mass movements, primarily landslides. A road network map was created using Google Earth imagery and extracted into a GIS layer to assess the impact of roads on landslides (Figure 6d).

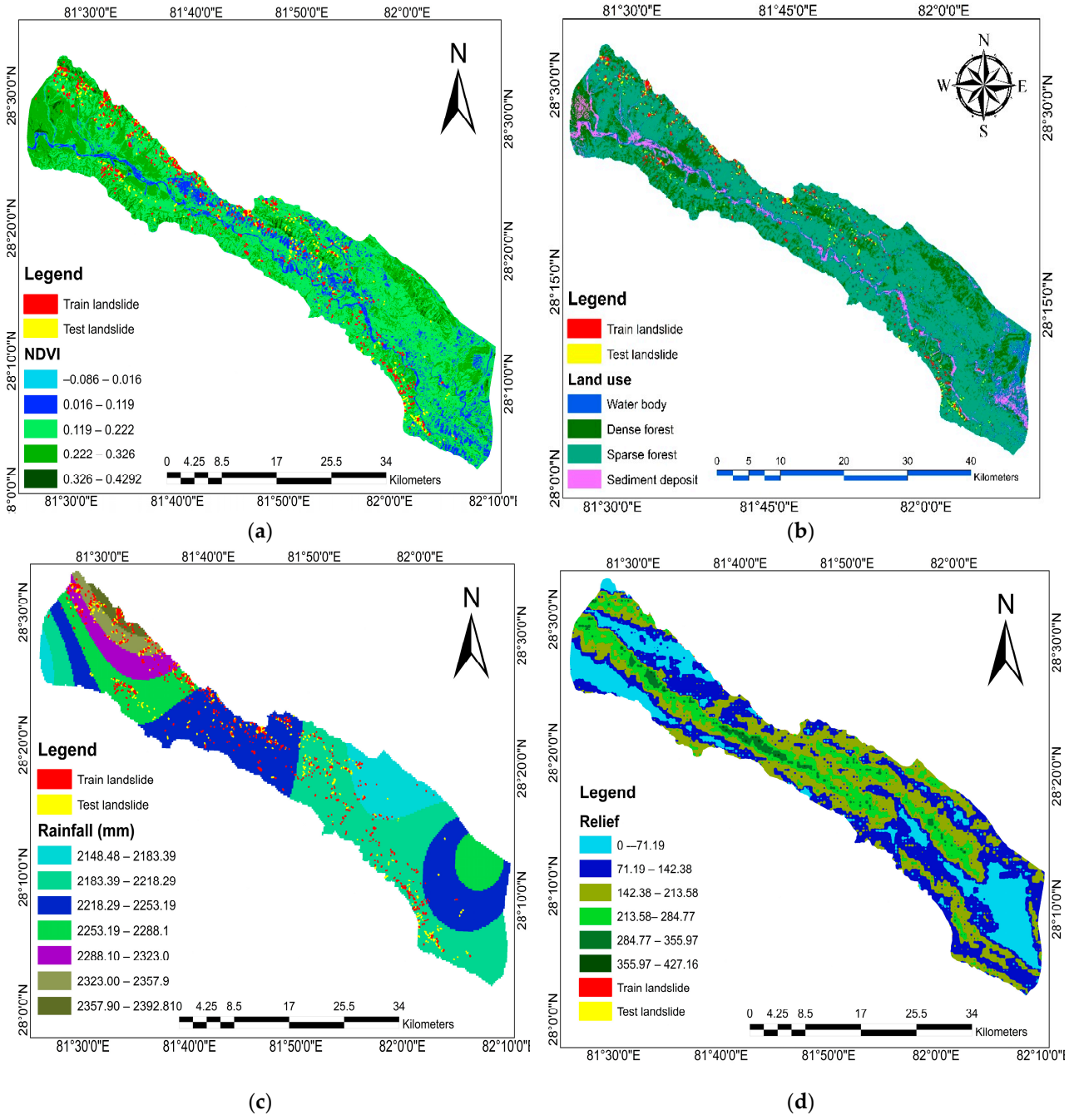

Figure 5. (**a**) NDVI map. (**b**) Land use map. (**c**) Rainfall map. (**d**) Relief map.

3.3. Multicollinearity Diagnostic

In order to create a landslide susceptibility map, 14 conditioning factors were considered. We took steps to minimize multicollinearity so that the model would be accurate and that duplicate variables would not have an effect to impact the result. Multicollinearity is the occurrence of high interrelation among two or more independent variables. The correlation between independent variables misleads the final result of prediction. To obtain better prediction for landslide susceptibility, the condition of multicollinearity should be avoided. To identify multicollinearity, the variance inflation factor (VIF) was employed. Problems with multicollinearity within the set of independent variables are the focus of the investigation [27]. The computation of the variance inflation factor is an excellent illustration of an efficient landslide causative independent variable.

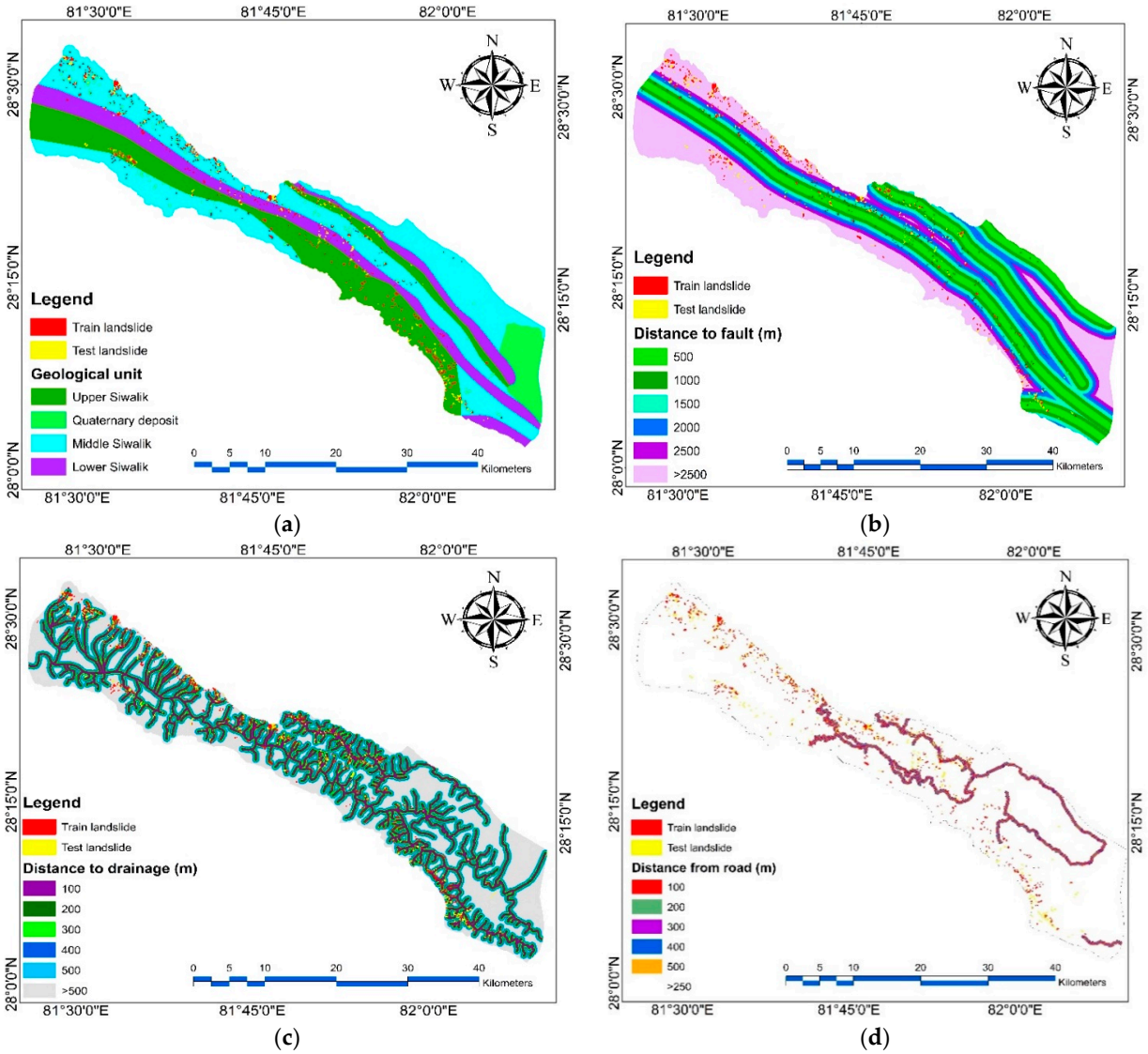

Figure 6. (**a**) Geological map. (**b**) Distance to fault map. (**c**) Distance to drainage. (**d**) Distance to road.

The evaluation of multicollinearity can be handled in several ways using different approaches when there are many independent variables. Academic discourse is incomplete without the concept of variables. Variance inflation factor (VIF_a) for a given variable X_a is computed using the method described by Vu et al. [28].

$$VIF_a = \frac{1}{1 - R_a^2}$$

The determination of the coefficient (R^2) shows how one variable (X_i) affects the other variables ($X_1, X_2, \ldots, X_{i-1}, X_{i+1}, \ldots, X_n$), and it can be any value between 0 and 1.

Hence, when the value of VIF_a is between 1 and 10, the amount of collinearity across variables is positively correlated with it. One may argue that, when $VIF_a = 1$, the variables in the dataset do not show multicollinearity. A VIF_a value between 1 and 5 shows less to moderate multicollinearity and a value greater than 5 indicates multicollinearity among the variables. When VIF_a is greater than 10 and R^2 is greater than 0.9, multicollinearity can significantly impact the anticipated performance of the model. Hence, we should eliminate the independent variable X_a [28]. A VIF_a value less than five is considered for the non-multicollinearity condition; hence, we set the threshold VIFa value at five in this study.

3.4. Susceptibility Model

For the landslide susceptibility analysis, four different bivariate models have been used: WoE, FR, SE, and IV models. The susceptibility analysis started with landslide inventory mapping. Past landslides were used as a guide for what might happen in the future. Landslides will occur in the future under the same factors, location, geology, slope, etc., that caused them in the past [29]. Over the study area, 1154 landslides were found and put on a map. A total of 70 percent of the landslides were used for training and 30% for testing. After making the landslide inventory map with training and testing data, the vector landslide data (polygons) were turned into a raster in GIS without changing the co-ordinates or the size of the pixels.

3.5. Weight of Evidence (WoE) Model

This model was initially created to examine mineral potential [30]. The weight of evidence method is a bivariate statistical technique that employs a log-linear Bayesian approach. This model calculates the likelihood of a landslide based on the contribution of evidence for slope instability [31]. Bonham-Carter [30] comprehensively describes vocabulary and mathematical derivations. The weight of evidence model assigns a weight to each landslide predicting factor based on the existence or absence of the landslide (L).

$$W^{+} = \ln \frac{P\left\{\frac{B}{L}\right\}}{P\left\{\frac{B}{L\prime}\right\}}$$

$$W_i = \ln \frac{P\left\{\frac{B\prime}{L}\right\}}{P\left\{\frac{B\prime}{L\prime}\right\}}$$

where:

ln is the log and P is probability;

B is the presence of a potential landslide factor;

B' is the absence of a potential landslide factor;

L and L' are the presence and absence of landslide, respectively.

W^{+} and W^{-} indicate the presence and absence of predictive variables, respectively. Similarly, W^{+} shows a positive correlation between a predictive variable and the landslide, whereas W^{-} shows a negative correlation between a predictive variable and the landslide.

After obtaining the W^{+} and W^{-} value, the weight contrast (C) was calculated by subtracting W^{-} from W^{+}. The weight contrast (C) gives the association between landslides and predictive variables.

The presence and absence of landslide in each predictive variable and their sub-class were obtained on a pixel basis. The formula was obtained in the modified form to calculate the pixel number.

$$W^{+} = \ln\left\{\frac{\frac{A1}{A1+A2}}{\frac{A3}{A3+A4}}\right\}$$

$$W^{-} = \ln\left\{\frac{\frac{A2}{A1+A2}}{\frac{A4}{A3+A4}}\right\}$$

where:

A_1 is the landslide pixels present on a given factor class;

A_2 is the landslide pixels absent in the given factor class;

A_3 is the pixels in the specified factor class that do not include any landslide pixels;

A_4 is the number of pixels in which neither landslide nor the given factors are present.

The obtained weight is further used to produce a contrast value for the particular susceptible variable, which is given by:

$$C = W^{+} - W^{-}$$

The obtained difference between weights (C) measures the strength of the correlation between the analyzed variable and landslides.

3.6. Frequency Ratio (FR) Model

When assessing landslide susceptibility using GIS methodologies and spatial data, the frequency ratio bivariate methodology is frequently used [21,28]. It is often and successfully utilized for mapping landslide susceptibility [32]. The landslide inventory map and factor map have been combined using the standard equation to determine the FR for each class of the causative components [33].

Numerous researchers have adopted this approach to study landslide susceptibility in the past and they have asserted that the FR model is a commonly used, highly accepted model with a high prediction rate. In this study, the frequency ratio is utilized to calculate the ratio of the number of pixels in the class to the entire number of pixels present in the study region, as well as the ratio of the pixels in the class to the total number of landslide pixels. The FR is the ratio of the area of the class as a percentage of the overall map to the number of landslides in the targeted class as a percentage of all landslides [34]. Total FR was determined for each factor after computing the FR value for each subclass. Each factor's final weighted value was determined. The final susceptibility map was created by overlaying the total weighted values with each factor in the GIS. Total FR values above one are thought to indicate high susceptibility, whereas values below 1 indicate low susceptibility. The frequency ratio computation process is illustrated below.

$$FR = \frac{\frac{A}{B}}{\frac{C}{D}}$$

where:

A is the number of landslide pixels for each factor.
B is the number of total landslide pixels in the study area.
C is the pixel number in the class area of each factor.
D is the total pixel in the study area and FR is the frequency ratio of a class for the factor.

3.7. Information Value (IV) Method

The information value model is a standard bivariate statistical method. This technique frequently forecasts the geographic link between landslides and factor classes [35]. Yin and Yan [36] created and adopted this model for the slope instability study. Sarkar et al. [35] improved the model further and attempted to make it more valid and precise.

The information value of each factor was determined using conditional and prior probability. First, the conditional probability was calculated by dividing the landslide pixel of each subclass by a single component of the pixel of this subclass. Similarly, the prior probability was calculated by dividing the total number of landslide pixels in the study region by the total number of pixels in the study area. The mathematical derivations and relations are available in Yin and Yan [36].

$$\text{Conditional probability } (Pc) = \frac{Si}{S}$$

$$\text{Prior probability } (Pp) = \frac{Ni}{N}$$

$$\text{Information Value } (IV) = \frac{Pc}{Pp}$$

where *Si* is the number of landslide pixels present in the subclass;
S is the pixel of the subclass;
Ni is the landslide pixel of the total area;
N is the pixel of the whole area.

3.8. Shannon's Entropy (SE) Method

SE model is derived from the frequency ratio model. The frequency ratio model does not consider the weightage of the causative factor [37]. The term entropy was adopted from the Boltzmann principle, which measures the disorder or uncertainty of a system [38]. In the present day, the entropy value is used to analyze natural hazards. In the case of a landslide, the entropy value gives the environment dissimilarity, which indicates the potential factors that cause a landslide. The index of entropy consists of the following procedures to calculate the weightage of causative factors:

$$P_{ab} = FR / \sum_{a=1}^{m} \mathrm{FR}$$

$$\sum_{a=1}^{m} \mathrm{Eab} = \sum_{k=0}^{n} (Pab) * (lnPab)$$

$$Hab = 1 + \sum_{a=1}^{m} \mathrm{Eab}$$

$$Wb = Hab / \sum_{a=1}^{m} Hab$$

Pab is the probability density and FR is the frequency ratio of sub-factors. *Wb* is the weightage of causative factors obtained from Shannon's entropy technique.

3.9. Validation of Susceptibility

We validated the results by using the receiver operating characteristic (ROC) curve. It is a tried and true approach for determining how accurately different algorithms are used to create landslide susceptibility maps [39]. Validation was carried out with the assistance of 30% of the testing data that were generated while preparing the landslide inventory map. The ROC curve is constructed with the help of a two-axis graph. On the Y axis, we could determine the true positive rate (sensitivity); on the X axis, we could evaluate the false positive rate (1-specificity). The AUC value is somewhere in the range of 0.5 and 1. In the case of percentage, AUC value ranges from 0 to 100%. A value greater than 50% indicates that the model can be accepted. The accuracy of the models is determined by examining the curve. The model with full accuracy for forecasting landslide susceptibility has an AUC value of 1 or 100%, whereas the weak model without useful information has an AUC value of 0.

4. Results

4.1. Multocollinearity Diagnostic

The VIF is employed to identify and address the issue of multicollinearity, which occurs when there is a high correlation between predictor variables. The VIFs of the 14 condition factors were estimated based on the 14 conditioning factor maps. The results are shown in Table 1. All condition factors have VIF values below 5, indicating their suitability for landslide susceptibility mapping.

Table 1. Variance inflation factor (VIF) of the 14 conditional factors.

Conditional Factors	X_1	X_2	X_3	X_4	X_5	X_6	X_7	X_8	X_9	X_{10}	X_{11}	X_{12}	X_{13}	X_{14}
VIF	1.5	4.6	5.5	2	1.9	1.5	1.8	3.4	2.3	1.5	5.6	3.7	2.5	4.2

Where X_1 is slope angle, X_2 is aspect, X_3 is plan curvature, X_4 is profile curvature, X_5 is geology, X_6 is NDVI, X_7 is land use, X_8 is TWI, X_9 is SPI, X_{10} is distance to road, X_{11} is distance to river, X_{12} is distance to fault, X_{13} is relative relief, and X_{14} is rainfall.

4.2. Landslide Susceptibility Analysis

Four bivariate models (WoE, SE, IV, and FR) were used to determine the spatial correlation between each factor contributing to landslides and the actual landslide locations. Table 2 presents the corresponding results. The assigned values for each factor in Table 2 are determined based on the observed landslides, including the percentage of pixels with the applied models. Certain factor classes exhibited elevated values across all four models.

Table 2. The statistics of landslide pixels and results obtained from FR, WoE, SE, and IV.

Factor	Class	Class (%)	Landslide (%)	FR	SE	WoE	IV
Rainfall (mm)	2148–2183	9.827	2.85	0.29	1.03	−0.56	−0.53
	2183–2218	34.227	21.87	0.64	1.05	−0.13	−0.19
	2218–2253	31.2	28.86	0.92	1.06	−0.05	−0.03
	2253–2288	13.98	9.74	0.69	1.06	−0.18	−0.15
	2288–2323	5.52	11.32	2.05	1.12	0.34	0.31
	2323–2357	4.73	11.69	2.46	1.13	0.55	0.5
	2357–2392	4.61	13.64	8.47	1.14	0.99	0.93
Land use	Water body	2.59	6.58	2.53	1.16	0.423	0.403
	Dense forest	18.18	2.58	2.14	1.03	−0.846	−0.846
	Sparse forest	72.23	63.9	3.82	1.31	−0.107	−0.05
	Sediment deposit	7.03	26.93	0.82	1.15	0.69	0.583
Aspect	N	6.241	2.21	0.35	1.06	−0.27	−0.45
	NE	17.52	3.37	0.31	1.05	0.56	−0.51
	E	4.9	2.17	0.43	1.07	−0.39	−0.36
	SE	17.3	24.82	1.42	1.13	1.32	0.15
	S	9.85	19.15	1.94	1.15	0.94	0.28
	SW	19.94	28.31	1.42	1.14	1.46	0.15
	W	10.1	10.8	1.06	1.12	0.66	0.02
	NW	14.05	7.21	0.51	1.07	0.61	−0.08
NDVI	−0.086–0.016	0.28	8.52	29.8	1.09	−1.03	1.417
	0.016–0.119	12.24	28.54	2.33	1.05	−0.39	0.37
	0.119–0.222	59.98	52.49	0.87	1.01	0.04	−0.05
	0.222–0.326	26.14	6.55	0.25	1	−1.15	−0.6
	0.326–0.429	0.01	3.89	296.77	1.04	−1.39	0.46
Profile curvature	Convex	7.108	13.45	1.87	1.15	0.34	0.27
	Plannar	53.71	33.11	0.61	1.12	0.03	−0.12
	Concave	37.22	53.43	1.43	1.16	0.37	0.04
Plan curvature	Convergence	7.49	16.77	2.24	1.143	0.39	0.34
	Plannar	60.22	50.72	0.84	1.141	−0.17	−0.07
	Divergence	32.28	32.5	1.01	1.049	0.004	0.002
Geology	Lower Siwalik	28.78	24.97	0.867	1.16	−0.08	−0.06
	Middle Siwalik	45.07	64.3	1.41	1.15	0.33	0.15
	Upper Sialik	19.92	10.73	0.54	1.14	−0.21	−0.27
	Quaternary deposits	5.62	0	0	1	−0.02	0
Slope (°)	<15	50.95	14.73	0.289	1.002	−0.78	−0.53
	15–30	41.08	42.46	1.033	1.007	0.02	0.01
	30–45	7.76	36.69	4.72	1.026	0.84	0.67
	45–60	0.2	6.004	29.94	1.09	1.53	1.476
	>60	0.003	0.1	29.6	1.004	3.07	2.471
TWI	2.79–6.79	65.97	84.65	1.28	1.15	0.74	0.11
	6.79–10.79	30.97	13.81	0.44	1.13	−0.79	−0.35
	10.79–14.79	2.96	1.5	0.51	1.14	−1.82	−0.29
	14.79–19.07	0.089	0.03	0.38	1.12	−3.46	−0.41

Table 2. *Cont.*

Factor	Class	Class (%)	Landslide (%)	FR	SE	WoE	IV
Distance to road (m)	<100	9.76	2.31	2.36	1.05	−0.63	−0.63
	100–200	9.47	1.31	2.19	1.07	−1.38	−0.86
	200–300	9.24	0.7	1.8	1.05	−2.75	−2.15
	300–400	8.94	0.63	1.45	1.05	−2.19	−1.15
	400–500	8.67	0.97	1.19	1.06	2.17	−0.9
	>500	53.09	94	0.29	1.09	1.19	0.24
Distance to river (m)	<100	9.76	23.07	2.63	1.15	−0.52	0.37
	100–200	9.47	20.76	2.19	1.14	−0.58	0.34
	200–300	9.24	16.67	1.8	1.13	−0.7	0.25
	300–400	8.94	13.01	1.45	1.12	−0.83	0.16
	400–500	8.67	10.33	1.19	1.11	−0.94	0.07
	>500	53.9	16.13	0.29	1.05	−0.73	−0.52
Distance to fault (m)	<500	16.73	8.48	0.51	1.09	−1.03	−0.29
	500–1000	15.99	7.95	0.49	1.177	−1.06	−0.3
	1000–1500	14.77	10.97	0.74	1.118	−0.91	−0.13
	1500–2000	13.38	10.19	0.76	1.147	−0.94	−0.12
	>2000	10.01	12.95	1.29	1.157	−0.83	0.11
Relief (m)	0–71.19	19.52	9.56	0.48	1.09	−0.977	−0.31
	71.19–142.38	33.16	31.41	0.94	1.132	−0.34	−0.02
	142.38–213.58	31.16	32.06	1.09	1.141	−0.28	0.03
	213.58–284.77	13.52	21.74	1.61	1.156	−0.557	0.21
	284.77–355.97	2.62	3.22	1.23	1.146	−1.48	0.089
	355.97–427.16	1.18	2	1.16	1.11	−1.28	0.06
SPI	−11.57–−5.57	0.054	3.35	61.8	1.013	−1.46	2.79
	−5.57–−0.73	0.062	8.28	12.5	1.033	−1.04	1.09
	−0.73–3.33	12.05	86.68	6.88	1.02	0.81	0.83
	3.33–6.41	86.75	1.67	0.02	1.0001	−1.77	−1.73

We looked at the relationship between conditioning factors and landslide locations using the FR, SE, WoE, and IV models. The frequency ratios of the sub-factors are represented in Table 2 and the susceptibility map for landslides that were derived using the frequency ratio model is shown in Figure 7. As a result, if the weight is positive and the value is high, the landslide condition is favorable, whereas if the weight is negative and the value is low, this indicates that the landslide condition is unfavorable. A considerable positive correlation exists between the total amount of rainfall and the area affected by landslides. The FR value increased to a higher level as the total amount of rain increased. The FR value of the water body and the area of sparse vegetation is higher. The FR value of the southern aspect is greater than that of the northern aspect. The southwest aspect provides the most potential in the FR value. The FR value is at its peak when the NDVI is the lowest and when it is the highest. A concave or convergent slope's FR value is much larger than a planar slope's.

Regarding its geology, the Middle Siwalik has a higher FR value than the Lower and Upper Siwalik. A statistically significant positive link exists between the hill slope and the FR value. The FR value rose higher as the hill slope became steeper. When the topographical wetness index is at its lowest, the FR value is at its highest. There is a negative relationship between the distance to the road and the FR value, which states that the FR value will grow when there is less distance between the road and the landslide. The stream power index and the FR value have a substantial positive correlation. Similarly, there is an inverse relationship between the distance to the river and the FR value. Near the fault plane, the FR value has increased. The value of the FR increased as the distance to the river decreased. The terrace, alluvium deposits, and plain lands are less susceptible, whereas forest areas are highly susceptible. Altogether, 21% of the area falls under a very high susceptible area, whereas 28% and 32% fall under high to medium susceptible areas.

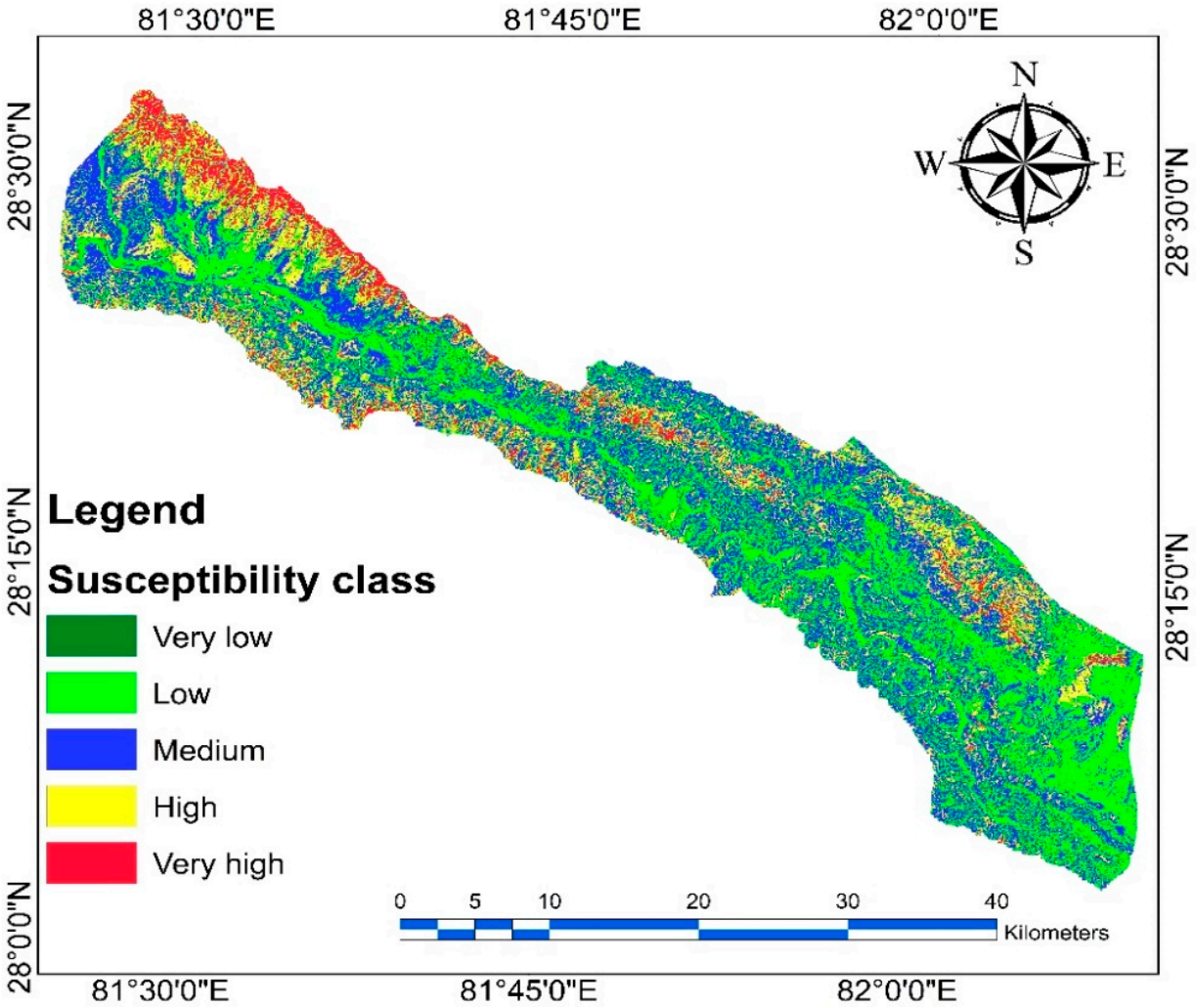

Figure 7. The landslide susceptibility distribution using the frequency ratio method.

The final landslide susceptibility map obtained using the weight of evidence model is shown in Figure 8. The result of the spatial relationship between landslides and conditioning factors is shown in Table 2. The WoE value is highest in the area with the highest rainfall. The old colluvium and alluvium have the highest WoE value. In the case of the slope, the WoE value is greatest at slopes greater than 60° and decreases as the slope decreases. The results show that the occurrence of landslides increases as the slope increases. The WoE value is highest at the SE and SW aspects. Landslides are more likely to occur in areas with a low topographical wetness index. Similarly, southern aspects are more susceptible to landslides. Landslides are very likely to occur in the Middle Siwalik.

The final landslide susceptibility map obtained using the information value method is shown in Figure 9. The information value analysis results show that landslide occurrence and rainfall amount are positively associated. The information value is higher in areas with higher rainfall. This model also showed that the southern aspect is more susceptible to landslides. Both convex and convergence slopes have a higher information value. The Middle Siwalik has a higher information value. Similarly, slope gradient and information value showed significant positive relationships. The lower topographical wetness index has a higher information value. Likewise, the information value increases as the stream power index decreases. The distance from rivers shows that the information value increased with decreasing distance from the river.

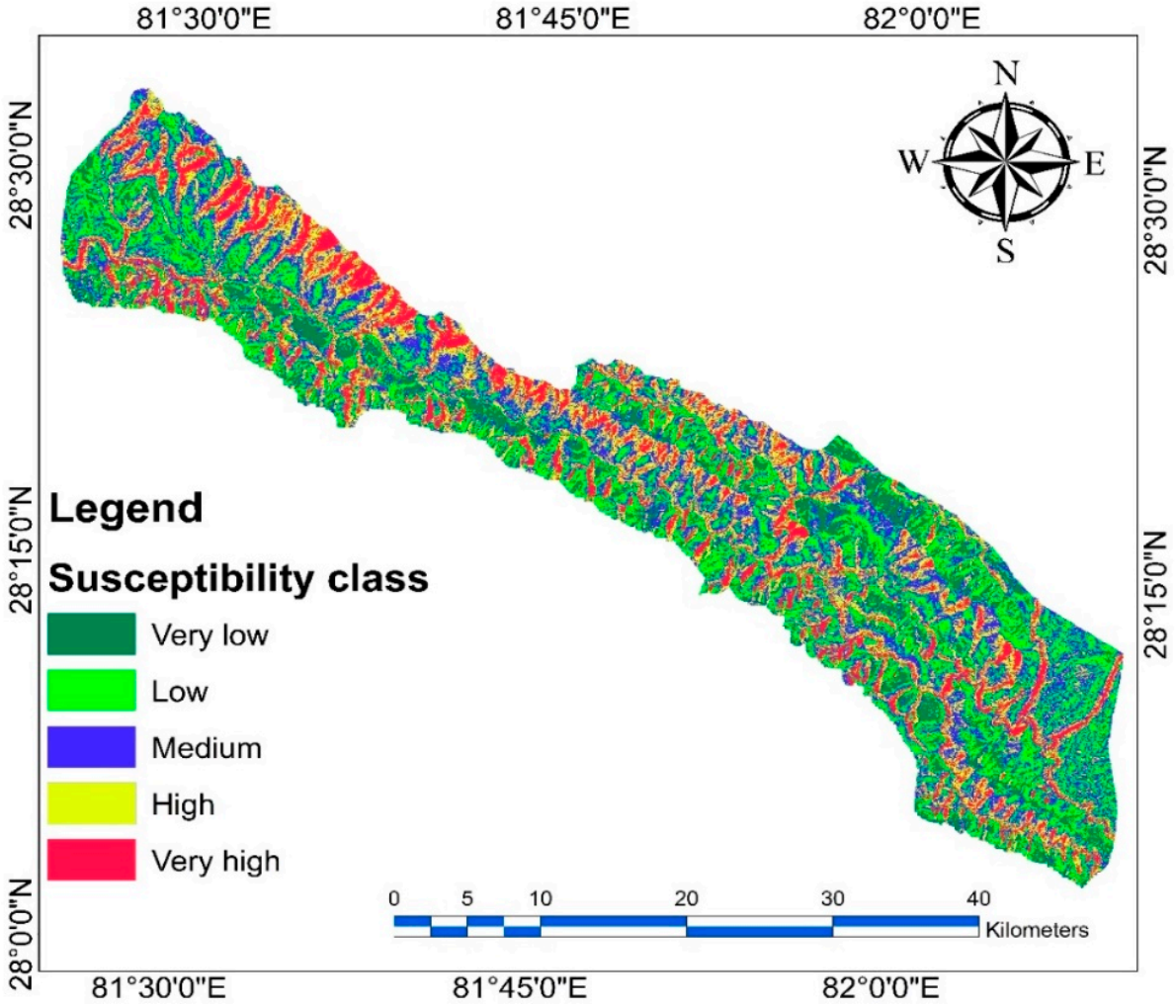

Figure 8. The landslide susceptibility distribution using the weight of evidence method.

Table 2 displays the relationship between landslide and conditioning factors according to the Shannon entropy model. The resulting map of landslide susceptibility is depicted in Figure 10. It indicates that land use significantly influences landslide occurrence, followed by precipitation, geology, profile curvature, and topographic wetness index. As seen in the preceding section, the P_{ab} value for Shannon entropy grows as rainfall quantity increases. Land use has the greatest entropy. For land use, colluvium, and alluvium, P_{ab} has a greater value.

Regarding geology, the likelihood of a landslide is greatest in the Lower Siwalik, followed by the Middle and Upper Siwalik. In terms of slope curvature, concave slopes are more susceptible to landslides. The hill slope greater than 15° is prone to landslides. In locations with a lower topographic wetness index, the P_{ab} value is greater. Similarly, the P_{ab} value is greatest (0.15 at 0–100 m and 1.048 at greater than 500 m) at a distance of 0–100 m. In terms of distance to fault, the P_{ab} value is greatest at a distance greater than 2000 m. The conclusion indicates that the hanging wall of the thrust is susceptible to developing a landslide.

The results of the susceptibility class were compared and presented in Figure 11. The percentage of very high susceptibility is obtained from the information value method, whereas the low susceptibility percentage is obtained from the Shannon entropy model. Medium susceptibility is obtained higher from the information value model, weight of evidence model, and frequency ratio model, whereas low susceptibility is obtained higher from the Shannon entropy method. The result shows that the susceptibility distribution is

more or less similar between frequency ratio, the weight of evidence, and the information value model; however, the Shannon entropy model has a slightly different result.

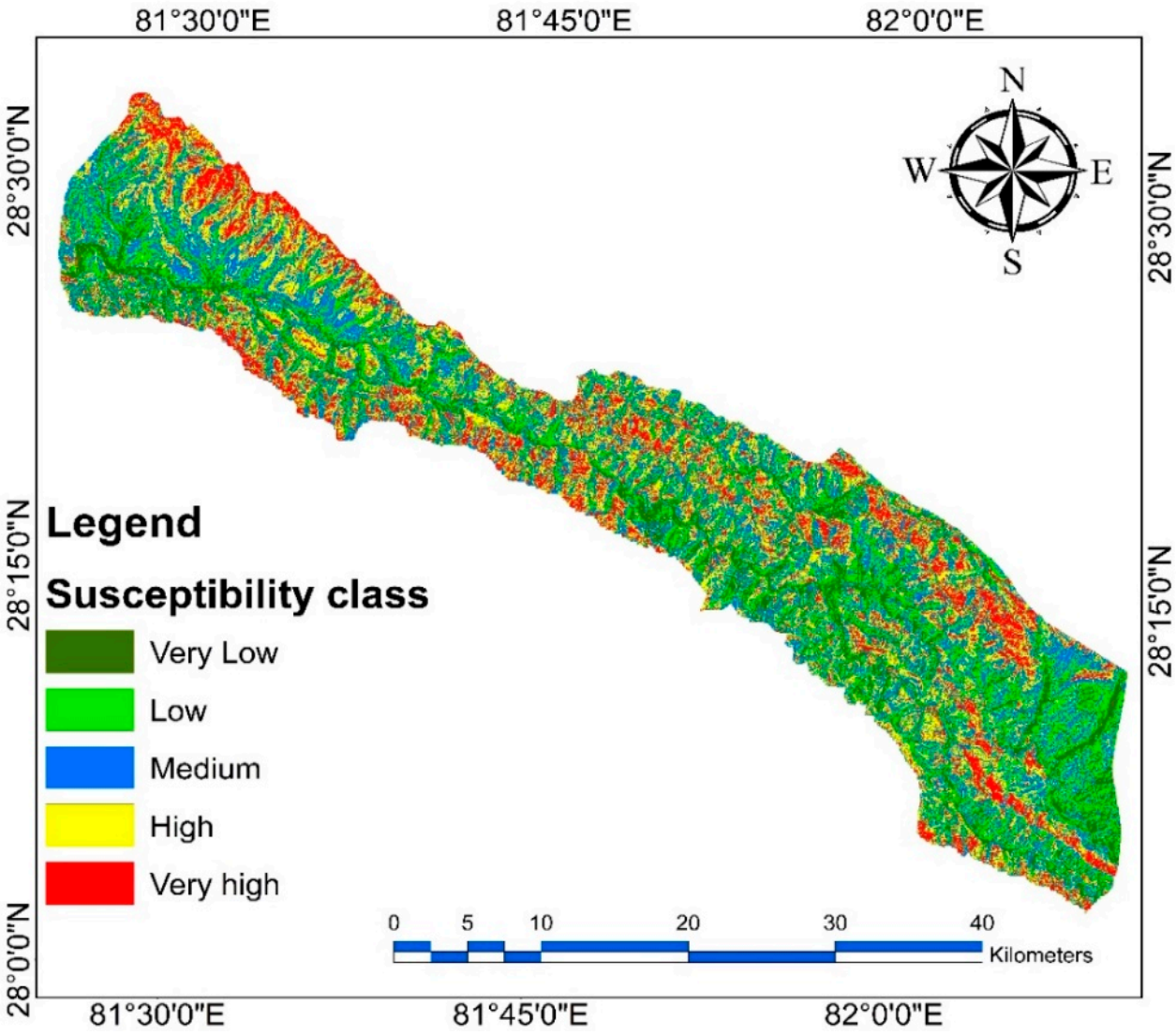

Figure 9. The landslide susceptibility distribution using the information value method.

4.3. Validation of the Susceptibility Maps

The success and prediction rate of all four models are shown in Figure 11. Validation datasets collected during fieldwork were used to verify the four landslide susceptibility models' predictions in this study. Figure 11 shows the performance of the model using the area under the curve (AUC). The results show that all four models are capable of accurately predicting susceptibility. Because of this, all four models demonstrated reasonable prediction: WoE (79.97%), FR (75.3%), SE (73.2%), and IV (74.4%). Similarly, the success rate of all four models is genuine and acceptable: WoE (85%), FR (78.75), SE (72.2%), and IV (78.57%). In terms of mapping landslide susceptibility in the study area, however, the WoE model scored the best with a 79.9% prediction and 85% success rate, while the SE model had the lowest prediction at 73.2% and lowest success rate at 72.2%. When it came to susceptibility modeling, the weight of the evidence demonstrated that the optimal model could integrate expert knowledge with field datasets.

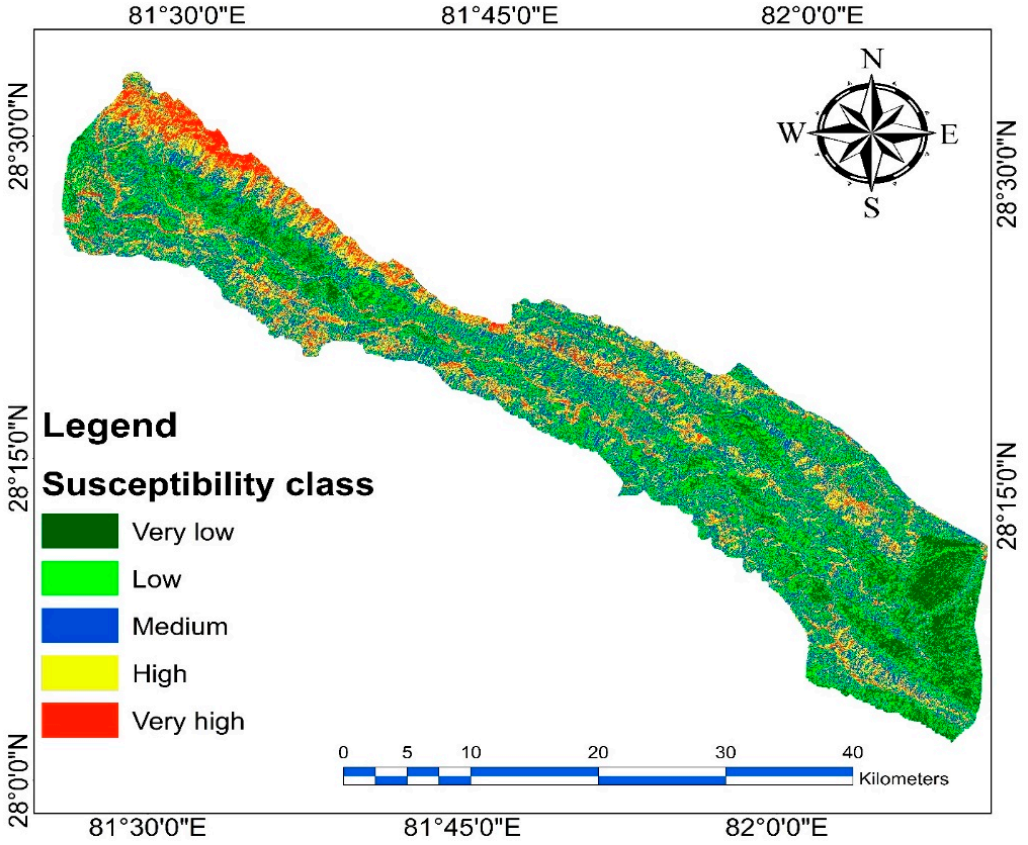

Figure 10. The landslide susceptibility distribution using the Shannon Entropy method.

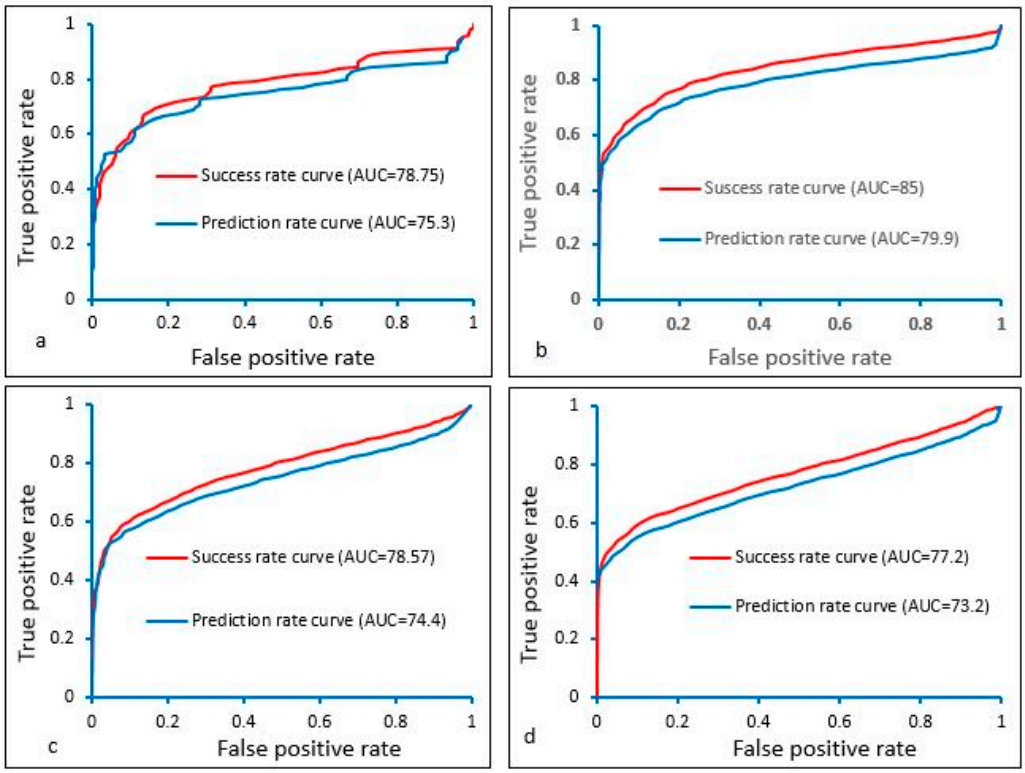

Figure 11. The area under curves shows the prediction rate of the susceptibility map produced by (**a**) FR, (**b**) WoE, (**c**) IV, and (**d**) SE models.

Figure 12 displays the areas covered by the five levels of susceptibility: very high, high, medium, low, and very low. According to the WoE model, 19% of the study area is occupied by the high susceptibility class. The study area is distributed as follows: 23% is highly susceptible, 26% is medium susceptible, 21% is low, and 11% has very low susceptibility. According to the FR model's landslide susceptibility map, 8% of the study area is classified as very low susceptibility. Similarly, 20% of the study area falls into the low susceptibility category, 32% into the medium susceptibility category, 22.7% into high susceptibility, and 18% into the very high susceptibility class. Very low susceptibility accounts for 27% of the study region and low susceptibility for 31%, according to the landslide susceptibility map generated using the SE model. The study area is moderately susceptible for 25% of the area, highly susceptible for 8%, and very highly susceptible for 9%. Based on IV model, 21% of the area is occupied by very high susceptibility, 17% by high susceptibility, 34% medium susceptibility, 19% by low susceptibility, and 9% by very low susceptibility class. Since all four models (FR, SE, WoE, and IV) generated respectable susceptibility maps, this comparison analysis proves that they are all viable methods for mapping landslides in Siwalik Hills of Nepal.

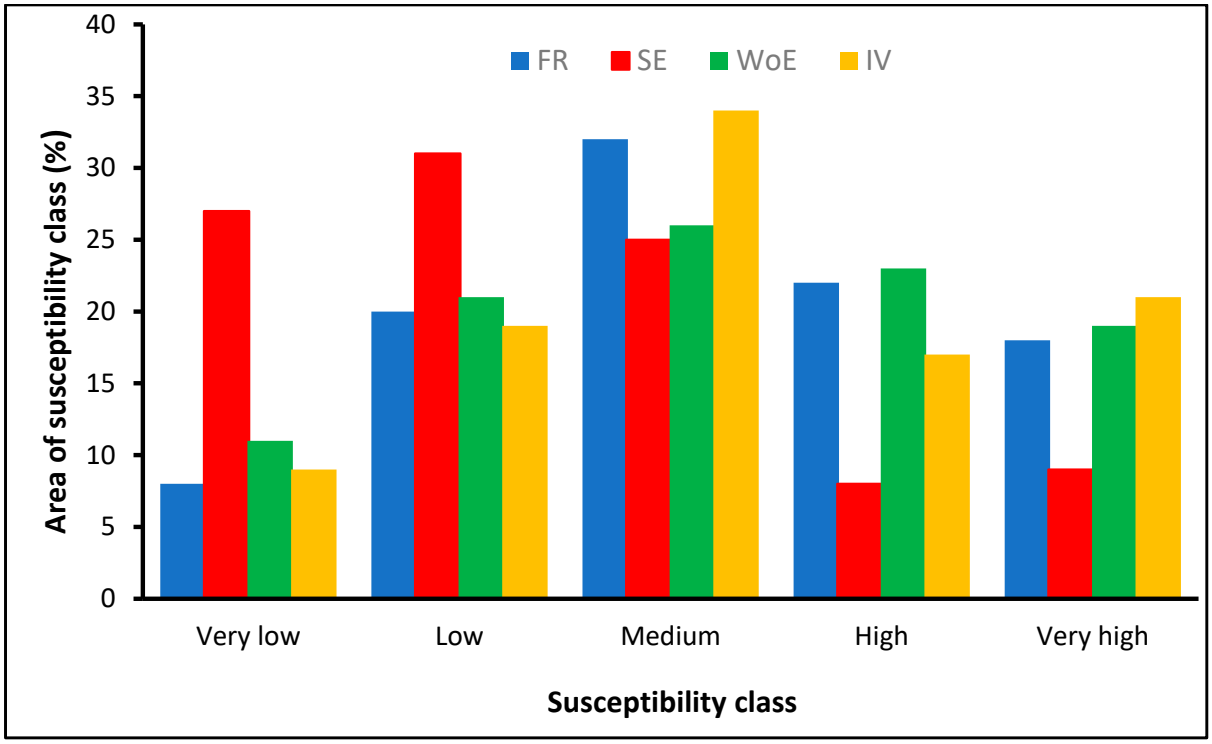

Figure 12. Landslide susceptibility class distribution of four different models.

5. Discussion

The purpose of this study was to compare four bivariate models of the geographic likelihood of landslide occurrence using FR, SE, WoE, and IV approaches, as well as to assess each causative element in landslide susceptibility. At last, we displayed maps of landslide susceptibility, which divide the region into discrete homogeneous zones with differing levels of susceptibility to landslides. An inventory of landslides and 14 weighted causal elements were integrated to create the four models. Every model has advantages of its own; the FR model is particularly simple to apply and previous study results are easily interpreted and widely acceptable [21,40]. One general approach for determining landslide susceptibility is the FR model. The WoE model is another well-known statistical method for mapping the likelihood of landslides. Based on the data regarding slope instability, this model determines the chance of a landslide [30]. The WoE model outperforms other models

in terms of landslide susceptibility prediction accuracy and ease of use [24]. A measure of a system's disorder or uncertainty, the Boltzmann principle [38], is the source of the term entropy. Natural disaster analysis now makes use of the entropy value. The environmental dissimilarity provided by the entropy value in a landslide scenario is indicative of the possible causes of the landslide. In this way, an established bivariate statistical approach is the information value model. According to Sarkar et al. [41] this method is commonly used for landslide factor class forecasting.

The training data for the four susceptibility models showed satisfactory goodness of fit. Nevertheless, there exist slight disparities among the models, with the WoE model exhibiting the higher level of conformity. This is evident from the AUC values of the ROC, which reaches 0.799. The success rate of the WoE model is 85% in this study. Choosing the elements that cause landslides is a crucial stage that significantly impacts the accuracy of a landslide susceptibility study. The fields of topography, geology, hydrology, and geomorphology are commonly employed in landslide susceptibility modeling.

This study utilized four approaches to assess the significance of the causal factors and the discrepancies observed among the data obtained from the four models employed. The Middle Siwalik formation, consisting of a thick layer of sandstone beds, exhibits the highest frequency of landslides. The Lower Siwalik formation, consisting of mudstone–shale layer ranks as the second highest. An ongoing rise in landslide density is evident in the parameter measuring the density of geological boundaries, indicating a strong association between the density of geological boundaries and the occurrence of landslides. The majority of landslides in the examined region are linked to slope angles greater than 15°; however, a slope greater than 30° is found as more susceptible for landslide. The study region consists of a smaller area (<12%) of steep slope (slope greater than 45°). The area of steep slope and area of landslide present show that the steep slope is highly susceptible for landslide. The western slope exhibits the most elevated concentration of landslides. Drainage networks have a detrimental impact on landslide susceptibility by eroding the base of the slope and saturating the slope material. This saturation also affects the stability of the surrounding material, leading to a decrease in slope stability [21]. Therefore, it is anticipated that an increased number of landslides would occur in slopes that are located near a stream network. The results of this study indicate that the highest frequency of landslides is linked to the category indicating a distance of below 200 m from the river network. The model values show that the landslides are concentrated far from the fault.

The road network was found to have the highest concentration of landslides within a distance of 200 m. This occurrence is anticipated, as the process of excavating road cuts diminishes the sideways reinforcement of the material and has the potential to initiate landslides. Furthermore, this process modifies the inherent topography and hydrological system. In this study, the FR and SE model show that up to 200 m distance is highly susceptible for landslide but the other two models show that 400–500 m is susceptible. It may be due to the topographical and geological variation in the study region. The three generated LS maps exhibit a high level of accuracy, with a prediction rate of more than 70%. The results clearly demonstrate that WoE exhibits superior accuracy, with an area under the curve (AUC) value of 0.799, in comparison to the FR, SE, and IV models, which had AUC values of 0.752, 0.744, and 0.732, respectively. The correlation between the training data and validation data about landslide occurrences demonstrates a satisfactory level of agreement. The majority of pixels that experienced landslides were classified as having a very high or high sensitivity in all four models.

Regmi et al. [42] utilized frequency ratio, weights of evidence, and statistical index models to compare landslide susceptibility mapping in the Central Nepal Himalaya region. According to the statistics, the FR model had the highest performance, with a success rate of 76.8% and a predicted accuracy of 75.4%. The FR model demonstrated a 75% success accuracy and a 70% forecast accuracy in a specific area of the Uttarakhand Himalaya, India, for landslide susceptibility assessment according to Pham et al. [19]. Regmi et al. [43] conducted a study that achieved a success accuracy of 83.31% and a prediction accuracy

of 78.58% for mapping the susceptibility of landslides in the Bhalubang–Shivapur Area in Mid-Western Nepal by utilizing the FR model. Both the study and the model used in the study demonstrated a relatively accurate ability to forecast the susceptibility of the study area to landslides. In a study conducted by [44] in Bhotang village development committee, Nepal, the AUC values for the FR model were determined to be 0.713 for validation, 0.725 for training, and 0.722 for the entire dataset. In the previous studies conducted in Nepal, individual FR and WoE provided a higher prediction rate. A lower number of studies have been conducted by comparing the models in the Nepal Himalaya. In some of the previous mentioned research, the FR model showed better performance. There is no distinct different prediction rate between the four models; however, the WoE model showed better performance in the case of success rate and prediction rate in the Siwalik Hills of Nepal.

Human actions are the most manageable and modifiable causes leading to landslides in Nepal [45]. Several landslides are happening along the roads and transportation corridors. The road's presence in mountainous terrains has led to an increased risk of landslides due to undercutting and several slope denudations. Landslides are concentrated in certain areas near major highways and newly developed country roads, leading to increased losses and damages. When trying to repair the damaged roadways, the alignment consistently moves towards the hillside, causing additional destabilization of the delicate colluvial slope [45,46]. Engineering works are typically conducted during dry seasons by modifying the slope and surface morphology. These conditions persist until the next rainy season or beyond but may become unstable due to excessive rainfall or other triggering events [47]. Furthermore, human activities such as mining and quarrying in the fragile mountain are exacerbating the hill slopes, which, in turn, speeds up the process of landslides. Manchado et al. [48] noticed a large number of human-induced landslides in Far-Western Nepal, where haphazard road construction is the major cause for landslide initiation. This study could not focus on the detail of the anthropogenic landslide mechanism; however, both natural and human intervention play a significant role for landslide initiation. Land use and distance to road are considered the anthropogenic factors. In the fragile Siwalik Hills, road construction and gravel/limestone mining are rapidly growing so that shallow landslides are occurring every year in the monsoon period. This study provided the potential landslide-susceptible area in the Babai River catchment. Before conducting mining, road construction, and any other engineering work, the stakeholders, local government, and related agencies can use this result. The land use planner, agriculture department, road department, and many other relevant agencies can make dialogue and discussion about the possible landslide-prone area; for that, they can use this result for road and other development sustainability.

6. Conclusions

The study area is prone to frequent landslides. The likelihood of landslides in the Babai River watershed of Siwalik zone was mapped using the WoE, FR, SE, and IV models in this investigation. No comparison has been made between the four models in the existing literature on landslide susceptibility research in the Siwalik region. In order to replicate the models, a landslide inventory map and 14 conditioning factor maps were utilized. The VIF was implicated to address the multicollinearity issues. The models' efficacy was, thus, assessed using ROC curves. This study revealed that the WOE model had the best success and prediction rate (85% and 79.9%) based on AUC, while the SE model had a lower success and prediction rate (77.2% and 73.2%). Nevertheless, the four models included in this work demonstrate potential techniques for analyzing landslide susceptibility in Siwalik Hills of Nepal. In comparison to the rest of the study area, the western region of the study area exhibited a higher susceptibility to landslides. The majority of the steep slopes are situated in the western part of the research region. The national pride project, "Bheri-Babai diversion project", is now underway in the study region. Various geo-environmental challenges such as landslides, debris flow, floods, and river damming are now occurring and may continue to emerge in the future. Road blockage is a significant problem in the region during the monsoon period, causing disruptions to the diversion project and other human activities.

Ultimately, land use planning and efforts to reduce landslide risk in similar areas with comparable terrain and environmental conditions should benefit from the findings of this study. This research aims to identify areas prone to landslides to enable the local authority to implement measures for landslide prevention and safe habitation. The results ultimately contribute to ensuring sustainable road, settlement, and other physical development in the sedimentary terrain of Nepal.

Author Contributions: Conceptualization: B.P.B. and S.D.; data curation: B.P.B.; methodology: B.P.B.; analysis: B.P.B.; supervision: S.D. and C.-Y.T.; writing—original draft: B.P.B., S.D. and C.-Y.T.; writing—review and editing: S.D. and C.-Y.T. All authors have read and agreed to the published version of the manuscript.

Funding: This research received no external funding.

Institutional Review Board Statement: Not applicable.

Informed Consent Statement: Not applicable.

Data Availability Statement: Data are contained within the article.

Acknowledgments: Researchers want to express our gratitude to the people of the Babai River catchment, who directly helped us during a field visit.

Conflicts of Interest: The authors declare no conflicts of interest.

References

1. Ali, S.A.; Parvin, F.; Vojteková, J.; Costache, R.; Linh, N.T.T.; Pham, Q.B.; Vojtek, M.; Gigović, L.; Ahmad, A.; Ghorbani, M.A. GIS-based landslide susceptibility modeling: A comparison between fuzzy multi-criteria and machine learning algorithms. *Geosci. Front.* **2021**, *12*, 857–876. [CrossRef]
2. Cruden, D.M.; Varnes, D.J. *Landslides: Investigation and Mitigation. Chapter 3-Landslide Types and Processes*; Transportation Research Board Special Report; Transportation Research Board: Washington, DC, USA, 1996.
3. Hussain, Y.; Cardenas-Soto, M.; Martino, S.; Moreira, C.; Borges, W.; Hamza, O.; Martinez-Carvajal, H. Multiple geophysical techniques for investigation and monitoring of Sobradinho landslide, Brazil. *Sustainability* **2019**, *11*, 6672. [CrossRef]
4. Gómez, D.; García, E.F.; Aristizábal, E. Spatial and temporal landslide distributions using global and open landslide databases. *Nat. Hazards* **2023**, *117*, 25–55. [CrossRef]
5. Ministry of Home Affairs (MoHA). *Nepal Disaster Report 2021*; Landslide Resilience Portal; MoHA: Kathmandu, Nepal, 2021.
6. KC, D.; Dangi, H.; Hu, L. Assessing landslide susceptibility in the northern stretch of Arun Tectonic Window, Nepal. *CivilEng* **2022**, *3*, 525–540. [CrossRef]
7. Dhakal, S. Geological divisions and associated hazards in Nepal. In *Contemporary Environmental Issues and Methods in Nepal*; Central Department of Environmental Science, Tribhuvan University Nepal: Kathmandu, Nepal, 2014; pp. 100–109.
8. Bhandari, B.P.; Dhakal, S. A multidisciplinary approach of landslide characterization: A case of the Siwalik zone of Nepal Himalaya. *J. Asian Earth Sci. X* **2021**, *5*, 100061. [CrossRef]
9. Brabb, E.E. Innovative approaches to landslide hazard mapping. In Proceedings of the 4th International Symposium on Landslides, Toronto, ON, Canada, 16–21 September 1984; Volume 1, pp. 307–324.
10. Van Den Eeckhaut, M.; Poesen, J.; Verstraeten, G.; Vanacker, V.; Moeyersons, J.; Nyssen, J.; Van Beek, L.P.H. The effectiveness of hillshade maps and expert knowledge in mapping old deep-seated landslides. *Geomorphology* **2005**, *67*, 351–363. [CrossRef]
11. Yilmaz, I. Landslide susceptibility mapping using frequency ratio, logistic regression, artificial neural networks and their comparison: A case study from Kat landslides (Tokat–Turkey). *Comput. Geosci.* **2009**, *35*, 1125–1138. [CrossRef]
12. Guzzetti, F.; Mondini, A.C.; Cardinali, M.; Fiorucci, F.; Santangelo, M.; Chang, K.T. Landslide inventory maps: New tools for an old problem. *Earth-Sci. Rev.* **2012**, *112*, 42–66. [CrossRef]
13. Bhandari, B.P.; Dhakal, S. Spatio-temporal dynamics of landslides in the sedimentary terrain: A case of Siwalik zone of Babai watershed, Nepal. *SN Appl. Sci.* **2020**, *2*, 1–17. [CrossRef]
14. Vakhshoori, V.; Pourghasemi, H.R.; Zare, M.; Blaschke, T. Landslide susceptibility mapping using GIS-based data mining algorithms. *Water* **2019**, *11*, 2292. [CrossRef]
15. Chen, W.; Xie, X.; Peng, J.; Shahabi, H.; Hong, H.; Bui, D.T.; Zhu, A.X. GIS-based landslide susceptibility evaluation using a novel hybrid integration approach of bivariate statistical based random forest method. *Catena* **2018**, *164*, 135–149. [CrossRef]
16. Akgun, A.; Kıncal, C.; Pradhan, B. Application of remote sensing data and GIS for landslide risk assessment as an environmental threat to Izmir city (West Turkey). *Environ. Monit. Assess.* **2012**, *184*, 5453–5470. [CrossRef]
17. Colkesen, I.; Sahin, E.K.; Kavzoglu, T. Susceptibility mapping of shallow landslides using kernel-based Gaussian process, support vector machines and logistic regression. *J. Afr. Earth Sci.* **2016**, *118*, 53–64. [CrossRef]

18. Shirzadi, A.; Soliamani, K.; Habibnejhad, M.; Kavian, A.; Chapi, K.; Shahabi, H.; Tien Bui, D. Novel GIS based machine learning algorithms for shallow landslide susceptibility mapping. *Sensors* **2018**, *18*, 3777. [CrossRef]
19. Pham, B.T.; Tien Bui, D.; Indra, P.; Dholakia, M. Landslide susceptibility assessment at a part of Uttarakhand Himalaya, India using GIS–based statistical approach of frequency ratio method. *Int. J. Eng. Res. Technol.* **2015**, *4*, 338–344.
20. Chen, W.; Zhang, S.; Li, R.; Shahabi, H. Performance evaluation of the GIS-based data mining techniques of best-first decision tree, random forest, and naïve Bayes tree for landslide susceptibility modeling. *Sci. Total Environ.* **2018**, *644*, 1006–1018. [CrossRef] [PubMed]
21. Ding, Q.; Chen, W.; Hong, H. Application of frequency ratio, weights of evidence and evidential belief function models in landslide susceptibility mapping. *Geocarto Int.* **2017**, *32*, 619–639. [CrossRef]
22. Pradhan, A.M.S.; Kim, Y.T. Relative effect method of landslide susceptibility zonation in weathered granite soil: A case study in Deokjeok-ri Creek, South Korea. *Nat. Hazards* **2014**, *72*, 1189–1217. [CrossRef]
23. García-Rodríguez, M.J.; Malpica, J.A.; Benito, B.; Díaz, M. Susceptibility assessment of earthquake-triggered landslides in El Salvador using logistic regression. *Geomorphology* **2008**, *95*, 172–191. [CrossRef]
24. Dahal, R.K.; Hasegawa, S.; Bhandary, N.P.; Poudel, P.P.; Nonomura, A.; Yatabe, R. A replication of landslide hazard mapping at catchment scale. *Geomat. Nat. Hazards Risk* **2012**, *3*, 161–192. [CrossRef]
25. Gorum, T.; Fan, X.; van Westen, C.J.; Huang, R.Q.; Xu, Q.; Tang, C.; Wang, G. Distribution pattern of earthquake-induced landslides triggered by the 12 May 2008 Wenchuan earthquake. *Geomorphology* **2011**, *133*, 152–167. [CrossRef]
26. Shafique, M.; van der Meijde, M.; Khan, M.A. A review of the 2005 Kashmir earthquake-induced landslides; from a remote sensing prospective. *J. Asian Earth Sci.* **2016**, *118*, 68–80. [CrossRef]
27. Akinwande, M.O.; Dikko, H.G.; Samson, A. Variance inflation factor: As a condition for the inclusion of suppressor variable(s) in regression analysis. *Open J. Stat.* **2015**, *50*, 754. [CrossRef]
28. Vu, D.H.; Muttaqi, K.M.; Agalgaonkar, A.P. A variance inflation factor and backward elimination based robust regression model for forecasting monthly electricity demand using climatic variables. *Appl. Energy* **2015**, *140*, 385–394. [CrossRef]
29. Lee, S.; Talib, J.A. Probabilistic landslide susceptibility and factor effect analysis. *Environ. Geol.* **2005**, *47*, 982–990. [CrossRef]
30. Bonham-Carter, G.F.; Agterberg, F.P.; Wright, D.F. Integration of geological datasets for gold exploration in Nova Scotia. *Digit. Geol. Geogr. Inf. Syst.* **1989**, *10*, 15–23.
31. Umar, Z.; Pradhan, B.; Ahmad, A.; Jebur, M.N.; Tehrany, M.S. Earthquake induced landslide susceptibility mapping using an integrated ensemble frequency ratio and logistic regression models in West Sumatera Province, Indonesia. *Catena* **2014**, *118*, 124–135. [CrossRef]
32. Wu, Y.; Li, W.; Wang, Q.; Liu, Q.; Yang, D.; Xing, M.; Yan, S. Landslide susceptibility assessment using frequency ratio, statistical index and certainty factor models for the Gangu County, China. *Arab. J. Geosci.* **2016**, *9*, 1–16. [CrossRef]
33. Mondal, S.; Maiti, R. Integrating the analytical hierarchy process (AHP) and the frequency ratio (FR) model in landslide susceptibility mapping of Shiv-khola watershed, Darjeeling Himalaya. *Int. J. Disaster Risk Sci.* **2013**, *4*, 200–212. [CrossRef]
34. Ehret, D.; Rohn, J.; Dumperth, C.; Eckstein, S.; Ernstberger, S.; Otte, K.; Rudolph, R.; Wiedenmann, J.; Xiang, W.; Bi, R. Frequency ratio analysis of mass movements in the Xiangxi catchment, Three Gorges Reservoir area, China. *J. Earth Sci.* **2010**, *21*, 824–834. [CrossRef]
35. Sarkar, S.; Roy, A.K.; Martha, T.R. Landslide susceptibility assessment using information value method in parts of the Darjeeling Himalayas. *J. Geol. Soc. India* **2013**, *82*, 351–362. [CrossRef]
36. Yin, K.L.; Yan, T.Z. Statistical prediction models for slope instability of metamorphosed rocks. In Proceedings of the 5th International Symposium on Landslides 1988, Lausanne, Switzerland, 10–15 July 1988; Volume 2, pp. 1269–1272.
37. Sharma, L.P.; Patel, N.; Ghose, M.K.; Debnath, P. Application of frequency ratio and likelihood ratio model for geo-spatial modelling of landslide hazard vulnerability assessment and zonation: A case study from the Sikkim Himalayas in India. *Geocarto Int.* **2014**, *29*, 128–146. [CrossRef]
38. Dam, N.D.; Amiri, M.; Al-Ansari, N.; Prakash, I.; Le, H.V.; Nguyen, H.B.T.; Pham, B.T. Evaluation of Shannon entropy and weights of evidence models in landslide susceptibility mapping for the Pithoragarh district of Uttarakhand state, India. *Adv. Civ. Eng.* **2022**, *2022*, 6645007. [CrossRef]
39. Panchal, S.; Srivastava, A.K. Expert based landslide susceptibility mapping for energy infrastructure planning. *J. Inf. Optim. Sci.* **2022**, *43*, 635–641. [CrossRef]
40. Demir, G.; Aytekin, M.; Akgün, A.; Ikizler, S.B.; Tatar, O. A comparison of landslide susceptibility mapping of the eastern part of the North Anatolian Fault Zone (Turkey) by likelihood-frequency ratio and analytic hierarchy process methods. *Nat. Hazards* **2013**, *65*, 1481–1506. [CrossRef]
41. Sarkar, S.; Kanungo, D.P.; Patra, A.K.; Kumar, P. GIS based spatial data analysis for landslide susceptibility mapping. *J. Mt. Sci.* **2008**, *5*, 52–62. [CrossRef]
42. Regmi, A.D.; Devkota, K.C.; Yoshida, K.; Pradhan, B.; Pourghasemi, H.R.; Kumamoto, T.; Akgun, A. Application of frequency ratio, statistical index, and weights-of-evidence models and their comparison in landslide susceptibility mapping in Central Nepal Himalaya. *Arab. J. Geosci.* **2013**, *7*, 725–742. [CrossRef]
43. Regmi, A.D.; Yoshida, K.; Pourghasemi, H.R.; Dhital, M.R.; Pradhan, B. Landslide susceptibility mapping along Bhalubang-Shiwapur area of Mid-Western Nepal using frequency ratio and conditional probability models. *J. Mt. Sci.* **2014**, *11*, 1266–1285. [CrossRef]

44. Acharya, T.D.; Yang, I.T.; Lee, D.H. GIS-based landslide susceptibility mapping of Bhotang, Nepal using frequency ratio and statistical index methods. *J. Korean Surv. Soc.* **2017**, *35*, 357–364.
45. Thapa, P.B. Occurrence of landslides in Nepal and their mitigation options. *J. Nepal Geol. Soc.* **2015**, *49*, 17–28. [CrossRef]
46. Adhikari, T.L. Landslide control and stabilization measures in Arniko Highway, central Nepal. In *Landslide Hazard Mitigation in the Hindu Kush-Himalayas*; Tianchi, L., Chalise, S.R., Upreti, B.N., Eds.; ICIMOD Publication: Lalitpur, Nepal, 2001; pp. 31–49.
47. Zhang, M.; Liu, J. Controlling factors of loess landslides in western China. *Environ. Earth Sci.* **2010**, *59*, 1671–1680. [CrossRef]
48. Manchado, M.T.; Allen, A.S.; Ballesteros-Canovas, J.A.; Dhakal, A.; Dhital, M.R.; Stoffel, M. Three decades of landslide activity in Western Nepal: New insights into trends and climate drivers. *Landslides* **2021**, *18*, 2001–2015. [CrossRef]